

RESEARCH ARTICLE | JULY 09 2025

Phase selection and texturing in molybdenum oxide films grown by reactive magnetron sputtering

Faezeh A. F. Lahiji ; Biplab Paul ; Grzegorz Greczynski ; Ganpati Ramanath ; Arnaud le Febvrier ; Per Eklund 

 Check for updates

Appl. Phys. Lett. 127, 011602 (2025)

<https://doi.org/10.1063/5.0273462>



View Online



Export Citation

Articles You May Be Interested In

Nanoscale friction of high entropy alloy sulfide thin films in comparison with molybdenum disulfide

Appl. Phys. Lett. (December 2023)

Formation of distorted rutile-type NbO₂, MoO₂, and WO₂ films by reactive sputtering

J. Appl. Phys. (February 2019)

Improvement of electrical and optical properties of molybdenum oxide thin films by ultralow pressure sputtering method

J. Vac. Sci. Technol. A (March 2012)

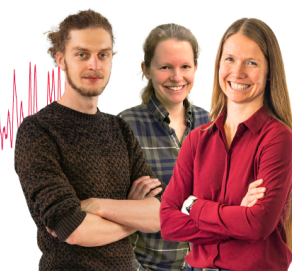
Webinar From Noise to Knowledge

May 13th – Register now



Zurich Instruments

Universität Konstanz



Phase selection and texturing in molybdenum oxide films grown by reactive magnetron sputtering

Cite as: Appl. Phys. Lett. **127**, 011602 (2025); doi: 10.1063/5.0273462

Submitted: 31 March 2025 · Accepted: 17 June 2025 ·

Published Online: 9 July 2025



View Online



Export Citation



CrossMark

Faezeh A. F. Lahiji,^{1,2,a)}  Biplab Paul,^{1,3}  Grzegorz Greczynski,¹  Ganpati Ramanath,^{1,2,4,5} 
Arnaud le Febvrier,²  and Per Eklund^{1,2,5} 

AFFILIATIONS

¹Thin Film Physics Division, Department of Physics, Chemistry and Biology (IFM), Linköping University, SE-58183 Linköping, Sweden

²Inorganic Chemistry, Department of Chemistry-Ångström Laboratory, Uppsala University, Box 538, SE-751 21 Uppsala, Sweden

³PLATIT AG, Eichholzstrasse 9, 2545 Selzach, Switzerland

⁴Department of Materials Science and Engineering, Rensselaer Polytechnic Institute, Troy, New York 12180, USA

⁵Wallenberg Initiative Materials Science for Sustainability, Department of Chemistry-Ångström Laboratory, Uppsala University, Box 538, SE-751 21 Uppsala, Sweden

^{a)} Author to whom correspondence should be addressed: faezeh.a.f.lahiji@kemi.uu.se

ABSTRACT

Molybdenum oxide films offer a rich variety of properties for diverse applications, but exclusive synthesis of desired phases is a major challenge. Here, we demonstrate that oxygen flow ratio $f_{O_2} = [O_2]/[Ar + O_2]$ is crucial not only for phase selection of non-layered monoclinic MoO₂ and layered orthorhombic α -MoO₃ but also for controlling grain size and preferred orientation. Both mica and sapphire support exclusive MoO₂ formation for $0.15 \leq f_{O_2} \leq 0.25$ at deposition temperatures $T_{dep} = 400$ and 500 °C, while α -MoO₃ forms only at $T_{dep} = 400$ °C for $0.35 \leq f_{O_2} \leq 0.5$. Within the f_{O_2} windows favoring each phase, high f_{O_2} fosters large grains with out-of-plane $0k0$ texture, except for MoO₂ on c-sapphire at $T_{dep} = 500$ °C, where no f_{O_2} -texture correlation is discernible. These findings provide a framework for rational synthesis of single-phase monoclinic MoO₂ and orthorhombic MoO₃ with control over texture and microstructure to access desired properties.

© 2025 Author(s). All article content, except where otherwise noted, is licensed under a Creative Commons Attribution (CC BY) license (<https://creativecommons.org/licenses/by/4.0/>). <https://doi.org/10.1063/5.0273462>

Molybdenum oxide thin films are attractive for a variety of applications in electro/photo-chromic coatings,^{1,2} resistive memories,^{3,4} displays,⁵ and gas sensing.⁶ Exclusive phase selection is crucial because optoelectronic properties⁷ depend on the Mo oxidation state and MoO_x stoichiometry but is a challenge because of the rich variety of phases and polymorphs in the Mo–O system. One can obtain multiple Mo_nO_{3n–1} Magnéli phases^{8,9} with $4 \leq n \leq 13$ ¹⁰ besides the monoclinic MoO₂^{8,9,11} and orthorhombic MoO₃,^{1,12} all of which offer vastly different properties. For instance, MoO₂ with Mo⁴⁺ is a metallic conductor while MoO₃ with Mo⁶⁺ is an optically transparent insulator. Molybdenum oxide films can be synthesized by many methods including wet-chemical routes,^{13–15} spray pyrolysis,¹⁶ and chemical¹⁷ and physical^{7,18,19} vapor deposition. Reactive gas flow ratio is known to be an important factor in phase selection, microstructure, and texture evolution,^{20–22} as shown for the reactive sputter deposition of metal

nitrides (e.g., using N₂ for TiN),^{23–26} carbides (e.g., using ethylene for TaC),^{27,28} and sulfides (e.g., using H₂S for VNbTaMoWS).^{29,30}

Here, we show that oxygen flow ratio $f_{O_2} = [O_2]/[Ar + O_2]$ is not only a key factor in the synthesis of single-phase films comprised of monoclinic MoO₂ or orthorhombic α -MoO₃ but also allows control over microstructure and grain orientation in these phases. We unveil conditions of preferential formation of monoclinic MoO₂ and orthorhombic α -MoO₃ at specific f_{O_2} ranges within $0.1 \leq f_{O_2} \leq 0.50$ on both mica and sapphire for two deposition temperatures, namely, $T_{dep} = 400$ and 500 °C. Within the exclusive phase formation windows, high f_{O_2} favors large grains and strong out-of-plane $0k0$ textures of monoclinic MoO₂ and orthorhombic α -MoO₃, compared to smaller low-textured grains at low f_{O_2} . These insights should pave the way for the exclusive synthesis of phase-selected MoO_x films with control over grain size and texture.

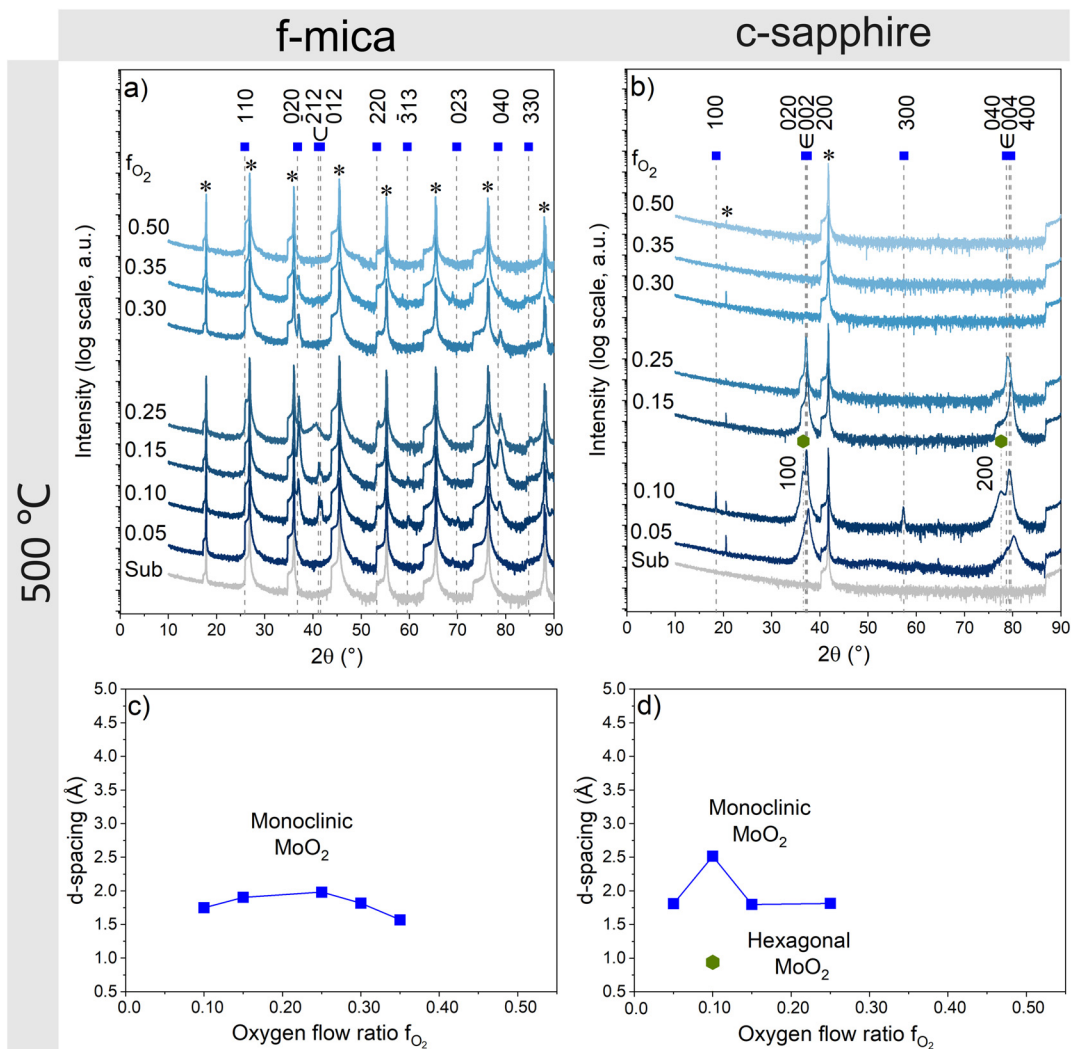


FIG. 1. X-ray diffractograms from MoO_3 films grown at $T_{\text{dep}} = 500^\circ\text{C}$ with $0.05 \leq f_{\text{O}_2} \leq 0.5$ on (a) f-mica and (b) c-sapphire showing Bragg peaks from monoclinic MoO_2 (blue squares), hexagonal MoO_2 (green hexagon) and the substrate (asterisks). Phase diagrams depicting MoO_2 formation on (c) f-mica and (d) c-sapphire vs f_{O_2} , with a representative d-spacing of the relevant phases plotted on the ordinate.

Molybdenum oxide thin films were grown using pulsed dc reactive magnetron sputter deposition from a 99.99% pure 50-mm-diameter Mo target from Plasmaterials. The Mo target was powered with bipolar pulsed dc voltage pulses at 150 W and 100 kHz with a 2 μs reverse time and 80% duty cycle to inhibit arcing. The substrates were $10 \times 10 \text{ mm}^2$ pieces of fluorphlogopite $\text{KMg}_3(\text{AlSi}_3\text{O}_{10})\text{F}_2(001)$ mica—referred henceforth as f-mica—purchased from Continental Trade, and c-plane sapphire(0001)—referred henceforth as c-sapphire—purchased from Alineason. The substrates were mounted on a rotatable sample holder in a 3×10^{-6} Pa base pressure UHV sputter-deposition chamber described elsewhere.³¹ Immediately prior to loading, fresh f-mica surfaces were exposed by scotch-tape exfoliation. Wet-chemical treatments were eschewed to obviate solvent intercalation and vacuum degradation. The c-sapphire substrates were

ultrasonicated successively in acetone and ethanol for 5 min each and blow-dried with N_2 .

Molybdenum oxide films were deposited by adjusting the oxygen flow ratio $f_{\text{O}_2} = [\text{O}_2]/[\text{Ar} + \text{O}_2]$ in the $0.05 \leq f_{\text{O}_2} \leq 0.50$ range. All depositions were carried out for 30 min at 2.5 mTorr pressure with total gas flow fixed at 60 ± 1.5 sccm. Prior to each deposition, the Mo target was sputter-cleaned at 1.7 mTorr Ar pressure at 150 W power for 2 min. The substrates were preheated to $T_{\text{dep}} = 400^\circ\text{C}$ or 500°C and held for 15 min for temperature homogenization.

Symmetric θ - 2θ x-ray diffraction (XRD) scans were acquired in a PANalytical X'Pert PRO diffractometer with a Cu K_α beam ($\lambda = 1.54 \text{ \AA}$) source operated at 45 kV and 40 mA. The incident optics include a 0.5° divergence slit, a 0.5° anti-scatter slit, and a Ni filter to minimize Cu K_β . The diffracted beam included a 5.0 mm anti-scatter

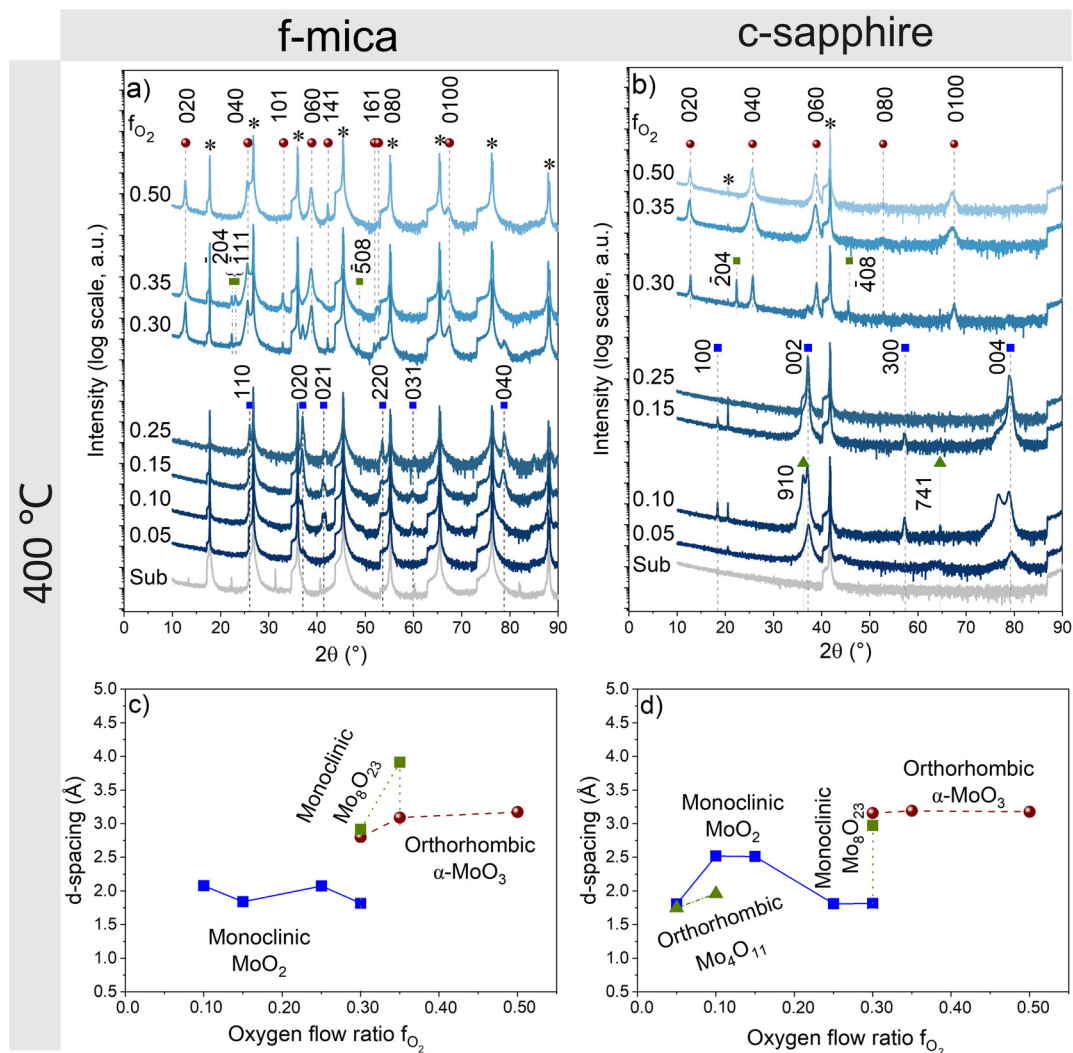


FIG. 2. X-ray diffractograms from MoO_x films grown at $T_{\text{dep}} = 400^\circ\text{C}$ with $0.05 \leq f_{\text{O}_2} \leq 0.5$ on (a) f-mica and (b) c-sapphire showing Bragg reflections from monoclinic MoO_2 (blue squares), orthorhombic $\alpha\text{-MoO}_3$ (red circles) and the substrates (asterisks). Phase diagrams depicting MoO_2 and MoO_3 formation as a function of oxygen flow ratio f_{O_2} on (c) f-mica and on (d) c-sapphire, with the ordinate plotting representative d -spacings of the relevant phases. Formation of traces of secondary monoclinic Mo_8O_{23} (green squares) and orthorhombic Mo_4O_{11} (green triangles) phases is also captured.

slit and 0.04 rad Soller slits. The PreFIX stage, equipped with an X'Celerator detector, was set to acquire data during θ - 2θ scans with a $0.0167^\circ/\text{step}$ size and equivalent time/step of 24.76 using the PIXcel 1D detector. Film thickness was estimated by x-ray reflectivity (XRR) measurements carried out in PANanalytical Empyrean diffractometer with similar Cu K_α characteristics, with a 0.5° divergence slit and hybrid mirror in the incident beam path and a 0.125° divergence slit in the diffracted beam optics.

Film morphology was characterized by a Leo 1550 Gemini, Zeiss scanning electron microscope (SEM) operated at 4 kV using in- and off-lens detectors to map Z-contrast and topography, respectively. Grain sizes were estimated from SEM micrographs by measuring the dimensions of 50 grains using the ImageJ 1.52n software and fitting the grain size distribution with a Gaussian.

X-ray photoelectron spectroscopy (XPS) was conducted to determine the oxidation state of Mo using a Kratos Analytical Axis Ultra DLD system with a monochromatic 1486.6 eV AlK_α source. The base pressure during measurements was 1.1×10^{-9} Torr (1.5×10^{-7} Pa). All spectra were recorded at 150 W anode power and normal emission angle. Setting a 20 eV analyzer pass energy results in a 0.55 eV full-width-half-maximum for the Ag $3d_{5/2}$ peak in a reference sample containing sputter-deposited Au, Ag, and Cu. The spectrometer calibration was verified by comparing Au $4f_{7/2}$, Ag $3d_{5/2}$, and Cu $2p_{3/2}$ positions to the recommended ISO standards for monochromatic Al K_α .^{32,33} The spectra were acquired over a $0.3 \times 0.7 \text{ mm}^2$ area and charge-referenced to the Fermi level $E_F = 0 \text{ eV}$.³⁴ We present results recorded from samples in the as-received state.

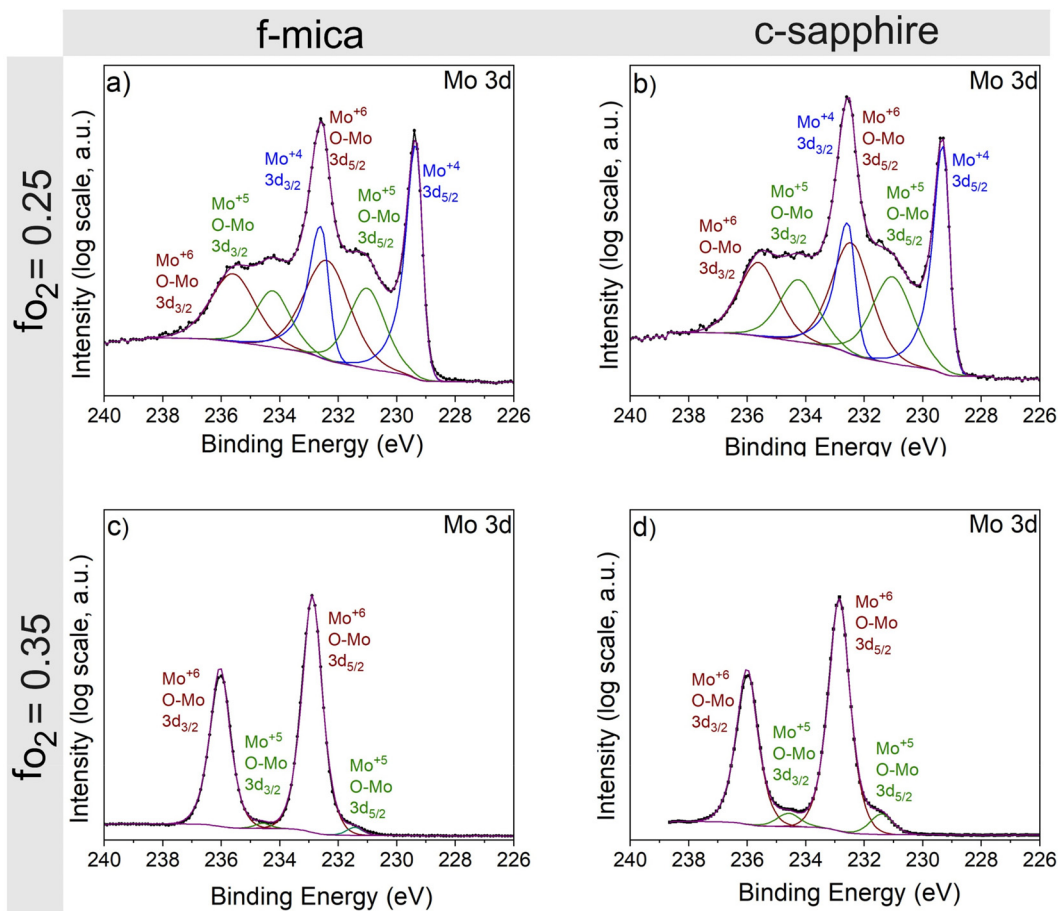


FIG. 3. Core-level Mo 3d spectra from XPS analyses of as-deposited MoO_x films grown at $T_{\text{dep}} = 400^\circ\text{C}$ on (a) f-mica and (b) c-sapphire with $f_{\text{O}_2} = 0.25$, and on (c) f-mica and (d) c-sapphire with $f_{\text{O}_2} = 0.35$.

Diffractograms from molybdenum oxide films deposited on f-mica [Fig. 1(a)] with the lowest $f_{\text{O}_2} = 0.05$ and the highest $f_{\text{O}_2} = 0.5$ exhibit only the $00l$ f-mica substrate peaks ($4 \leq l \leq 14$), suggesting amorphous MoO_x formation. Multiple Bragg reflections from monoclinic MoO_2 ⁸ were detected for $0.1 \leq f_{\text{O}_2} \leq 0.35$ with relative intensities varying with f_{O_2} . For $f_{\text{O}_2} = 0.30$ and 0.35 , only the 020 and 040 MoO_2 peaks are seen, indicating that the $0k0$ planes in monoclinic MoO_2 crystals are preferentially aligned with $00l$ planes in f-mica. The lack of crystalline phase formation at high f_{O_2} is likely due to oxygen-poisoning of the Mo target.^{35–37}

Diffractograms from films on c-sapphire [Fig. 1(b)] show monoclinic MoO_2 formation for $0.05 \leq f_{\text{O}_2} \leq 0.25$. Outside this range, the exclusive presence of $00l$ c-sapphire reflections suggests possible amorphous MoO_x formation. For $f_{\text{O}_2} = 0.05$, only the $00l$ and $0k0$ reflections from MoO_2 are seen, suggesting exclusive phase formation. An additional peak from hexagonal MoO_2 ³⁸ detected at $f_{\text{O}_2} = 0.1$, underscores the sensitivity of phase selection to oxygen flow. The one-dimensional phase diagram with representative interplanar spacings of MoO_x phases formed plotted vs f_{O_2} [see Figs. 1(c) and 1(d)] shows that monoclinic MoO_2 is exclusively favored on f-mica for $0.1 \leq f_{\text{O}_2} \leq 0.35$, and on c-sapphire for

$0.05 \leq f_{\text{O}_2} \leq 0.25$. However, at $f_{\text{O}_2} = 0.1$, distinct diffraction peaks corresponding to hexagonal MoO_2 are observed.

At $T_{\text{dep}} = 400^\circ\text{C}$, the films grown on f-mica [Fig. 2(a)] at $f_{\text{O}_2} = 0.05$ show no detectable MoO_x reflections, suggesting possible amorphous MoO_x formation, reminiscent of the behavior at $T_{\text{dep}} = 500^\circ\text{C}$. The $0k0$, $0kl$, and $hk0$ Bragg reflections from monoclinic MoO_2 are observed for $0.1 \leq f_{\text{O}_2} \leq 0.25$, indicating exclusive phase selection. For $f_{\text{O}_2} = 0.30$, three phases are observed: monoclinic MoO_2 indicated by the $0k0$ reflections, traces of monoclinic Mo_8O_{23} ³⁹ specified by the $h0l$ reflection, and orthorhombic α - MoO_3 ⁴⁰ indicated by hkl , $0k0$, and $h0l$ peaks. At $f_{\text{O}_2} = 0.35$, only orthorhombic α - MoO_3 peaks are detected for $0.35 < f_{\text{O}_2} \leq 0.5$.

Except for minor differences, MoO_x films grown on c-sapphire at 400 and 500°C show similar behaviors. For $0.05 \leq f_{\text{O}_2} \leq 0.1$, we predominantly observe $00l$ and $h00$ peaks from monoclinic MoO_2 [Fig. 2(b)] together with traces of $hk0$ and hkl reflections from orthorhombic Mo_4O_{11} .⁴¹ At $f_{\text{O}_2} = 0.1$, we observe an additional unindexed peak at $2\theta = 76.64^\circ$ not associated with known MoO_x phases. For $0.15 < f_{\text{O}_2} \leq 0.25$, we exclusively observe monoclinic MoO_2 .

At $f_{\text{O}_2} = 0.3$, orthorhombic MoO_3 and monoclinic Mo_8O_{23} are observed with traces of monoclinic MoO_2 similar to that seen on f-mica. Only orthorhombic MoO_3 forms for $0.35 \leq f_{\text{O}_2} \leq 0.5$.

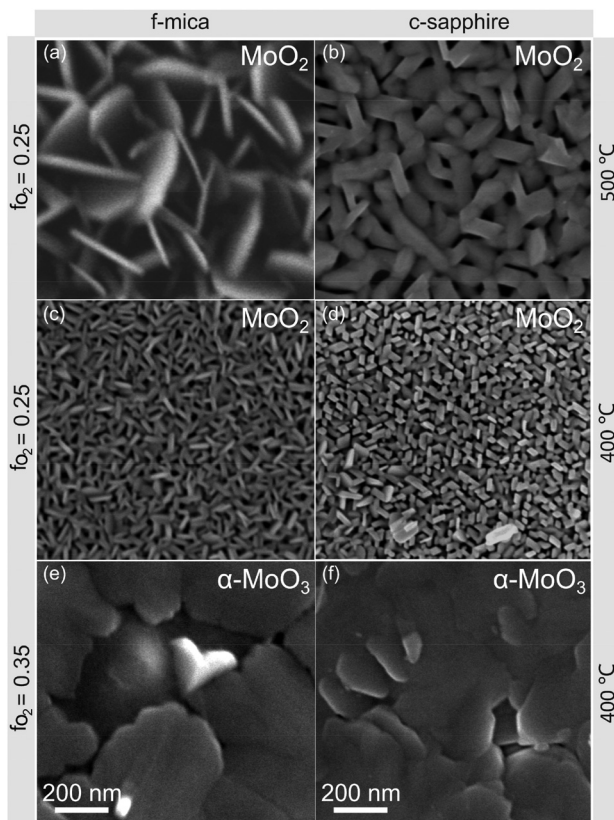


FIG. 5. SEM micrographs from films with either exclusive monoclinic MoO₂ or orthorhombic MoO₃ phases obtained at specific f_{O_2} - T_{dep} combinations on f-mica and c-sapphire.

020 MoO₂ reflection intensities continue to increase with f_{O_2} for $0.30 \leq f_{O_2} \leq 0.35$. The trends are similar for $T_{dep} = 400$ °C [Fig. 4(b)] but are somewhat obscured by the presence of additional phases. The f_{O_2} -driven accentuation of out-of-plane 020 texture indicates the tendency of 020 planes in the MoO₂ crystals to align with f-mica $00l$.

MoO₂ films on c-sapphire show no T_{dep} - f_{O_2} windows with texture- f_{O_2} correlations. Films grown at $T_{dep} = 500$ °C [Fig. 4(c)] feature dominant 002 MoO₂ reflections for $f_{O_2} = 0.05$ and $f_{O_2} = 0.1$, with smaller 020 MoO₂. Higher $f_{O_2} = 0.15$ and $f_{O_2} = 0.25$ result in solitary 200 and 002 peaks, respectively. Films grown at $T_{dep} = 400$ °C [Fig. 4(d)] with $f_{O_2} = 0.05$ and 0.25 showing solitary 002 and 020 peaks. The 002 peak dominates over smaller 100 reflection for $f_{O_2} = 0.1$ and 0.15 .

Orthorhombic α -MoO₃ films deposited with $0.30 \leq f_{O_2} \leq 0.50$ at 400 °C show a strong out-of-plane $0k0$ texture on both f-mica [Fig. 4(b)] and c-sapphire [Fig. 4(d)]. Out-of-plane 020 texture indicates the tendency of the b axis of the α -MoO₃ crystals to orient along the surface normal of both f-mica and c-sapphire substrates. The monotonic increase in the $0k0$ α -MoO₃ intensity for films on c-sapphire for $0.30 \leq f_{O_2} \leq 0.5$ indicates enhanced $0k0$ texturing with increasing f_{O_2} .

The above-mentioned results collectively indicate that high f_{O_2} correlates with higher $0k0$ textures in MoO₂ on f-mica and MoO₃ films

on both f-mica and c-sapphire for f_{O_2} - T_{dep} windows of exclusive formation of these phases. These texture- f_{O_2} correlations seen for these phase-substrate combinations are valuable for tailoring texture by adjusting f_{O_2} .

Films exclusively containing either MoO₂ or MoO₃ phases exhibit distinctive microstructures on f-mica and c-sapphire. While the MoO₂ microstructure was sensitive to both the substrate and T_{dep} , nearly identical MoO₃ microstructures were obtained on both substrates. Monoclinic MoO₂ films on f-mica at $T_{dep} = 500$ °C and $f_{O_2} = 0.25$ reveal ≈ 190 -nm-sized plate-shaped grains with ≈ 25 -nm-thick plate edges-oriented outward from the surface plane [Fig. 5(a)]. These plate-shaped grains are distinguished from the prism-shaped MoO₂ grains observed c-sapphire [Fig. 5(b)], which appear as coarser, anisotropic ≈ 34 -nm-wide and ≈ 130 -nm-long structures merging with each other, similar to the morphology reported for sputter-deposited MoO₂ films on c-sapphire.⁴⁸ At $T_{dep} = 400$ °C for the same $f_{O_2} = 0.25$, MoO₂ films on both f-mica and c-sapphire exhibit similar microstructures [Figs. 5(c) and 5(d)] with finer grain sizes than seen at $T_{dep} = 500$ °C. In particular, the plate-shaped grains of MoO₂ on f-mica are ~ 16 nm wide and ≈ 57 nm thick, while the prism-shaped MoO₂ crystals c-sapphire are ≈ 24 nm wide and ≈ 70 nm long. The finer grain structure at lower T_{dep} is consistent with decreased surface adatom mobilities and diffusion distances during film growth.

Orthorhombic α -MoO₃ films obtained at $f_{O_2} = 0.35$ consist of large 200–600-nm-wide sheet-shaped grains on both substrates [Figs. 5(e) and 5(f)]. These sheet-shaped grains differ from the MoO₂ plate-shaped grains in both scale and aspect ratio. While both feature flat morphologies with an out-of-plane $0k0$ texture, the α -MoO₃ sheets are substantially broader and flatter, forming extensive two-dimensional structures across the surface.

These microstructures of MoO₂ and MoO₃ featuring distinctively shaped crystals point to the connection between crystal shape and preferred orientation. For instance, the out-of-plane $0k0$ MoO₂ texture on f-mica indicates a preference for $0k0$ planes to stack along the thinnest dimension of the plate-shaped grains. The prism-shaped grains in MoO₂ films on c-sapphire correlate with the presence of prominent $h00$ and $00l$ peaks. The large flat sheets of α -MoO₃ are consistent with a strong out-of-plane $0k0$ texture on both substrates.

In summary, the oxygen flow ratio f_{O_2} is a key factor in determining the phase selection, texture, and microstructure of MoO_x films grown on f-mica and c-sapphire by reactive magnetron sputtering. Single-phase monoclinic MoO₂ and orthorhombic α -MoO₃ films can be exclusively obtained by adjusting f_{O_2} and T_{dep} . Specifically, MoO₂ forms at both $T_{dep} = 400$ °C and $T_{dep} = 500$ °C at low f_{O_2} , and α -MoO₃ forms only at $T_{dep} = 400$ °C at high f_{O_2} . Within the f_{O_2} windows of exclusive formation of MoO₂ and α -MoO₃ films, higher f_{O_2} fosters $0k0$ texture, except for MoO₂ films on c-sapphire that show no systematic f_{O_2} -texture correlation. These findings provide a framework for the synthesis of single-phase monoclinic MoO₂ and orthorhombic MoO₃ with control over texture and microstructure.

The authors acknowledge funding from the Swedish Government Strategic Research Area in Materials Science on Functional Materials at Linköping University (Faculty Grant SFO-Mat-LiU No. 2009 00971), the Knut and Alice Wallenberg foundation through the Wallenberg Academy Fellows program (KAW-2020.0196), the Swedish Research Council (VR) under Project No. 2021-03826, and the Swedish Energy

Agency under Project No. 52740-1. This work was partially supported by the Wallenberg Initiative Materials Science for Sustainability (WISE) funded by the Knut and Alice Wallenberg Foundation, and the U.S. National Science Foundation grant CMMI 2135725 through the BRITE program.

AUTHOR DECLARATIONS

Conflict of Interest

The authors have no conflicts to disclose.

Author Contributions

Faezeh A. F. Lahiji: Conceptualization (lead); Data curation (lead); Formal analysis (lead); Investigation (lead); Methodology (lead); Project administration (lead); Validation (lead); Visualization (lead); Writing – original draft (lead); Writing – review & editing (lead). **Biplab Paul:** Conceptualization (supporting); Data curation (supporting); Methodology (supporting); Supervision (equal); Validation (equal); Visualization (equal); Writing – review & editing (supporting). **Grzegorz Greczynski:** Data curation (equal); Formal analysis (equal); Investigation (supporting); Methodology (supporting); Software (equal); Validation (supporting); Visualization (supporting); Writing – review & editing (supporting). **Ganpati Ramanath:** Conceptualization (supporting); Data curation (supporting); Funding acquisition (supporting); Investigation (supporting); Methodology (supporting); Project administration (supporting); Validation (supporting); Visualization (supporting); Writing – review & editing (supporting). **Arnaud le Febvrier:** Conceptualization (supporting); Data curation (supporting); Investigation (supporting); Methodology (supporting); Project administration (supporting); Supervision (equal); Validation (supporting); Visualization (supporting); Writing – review & editing (supporting). **Per Eklund:** Conceptualization (equal); Data curation (equal); Funding acquisition (equal); Investigation (equal); Methodology (equal); Project administration (equal); Resources (equal); Supervision (equal); Validation (equal); Visualization (equal); Writing – review & editing (equal).

DATA AVAILABILITY

The data that support the findings of this study are available within the article.

REFERENCES

- M. R. Tubbs, “MoO₃ layers—Optical properties, colour centres, and holographic recording,” *Phys. Status Solidi A* **21**, 253–260 (1974).
- J. Scarminio, A. Lourenço, and A. Gorenstein, “Electrochromism and photochromism in amorphous molybdenum oxide films,” *Thin Solid Films* **302**, 66–70 (1997).
- A. Rasool, R. Amiruddin, I. R. Mohamed, and M. C. S. Kumar, “Fabrication and characterization of resistive random access memory (ReRAM) devices using molybdenum trioxide (MoO₃) as switching layer,” *Superlattices Microstruct.* **147**, 106682 (2020).
- M. Arita, H. Kaji, T. Fujii, and Y. Takahashi, “Resistance switching properties of molybdenum oxide films,” *Thin Solid Films* **520**, 4762–4767 (2012).
- V. K. Sabhapathi, O. Md. Hussain, P. S. Reddy, K. T. R. Reddy, S. Uthanna, B. S. Naidu, and P. J. Reddy, “Optical absorption studies in molybdenum trioxide thin films,” *Phys. Status Solidi A* **148**, 167–173 (1995).
- D. Mutschall, K. Holzner, and E. Obermeier, “Sputtered molybdenum oxide thin films for NH₃ detection,” *Sens. Actuators, B* **36**, 320–324 (1996).
- A. A. Al-Muntaser, M. A. Nasher, and M. M. Makhlof, “Structural, electrical, and linear/nonlinear optical characteristics of thermally evaporated molybdenum oxide thin films,” *Ceram. Int.* **48**, 8069–8080 (2022).
- A. Magnéli, G. Andersson, and G. Sundkvist, “On the MoO₂ structure type,” *Acta Chem. Scand.* **9**, 1378–1381 (1955).
- A. Magnéli, B.-H. Ansson, L. Kihlberg, and G. Sundkvist, “Studies on molybdenum and molybdenum wolfram oxides of the homologous series Me_nO_{3n-1},” *Acta Chem. Scand.* **9**, 1382–1390 (1955).
- Y. Bando, Y. Kato, and T. Takada, “Crystal growth of molybdenum oxides by chemical transport,” *Bull. Inst. Chem. Res., Kyoto Univ.* **54**, 330–334 (1976).
- P. Bakhru, “Equilibria between MoO₂ and liquid molybdenum oxide,” Master thesis (University of Missouri-Rolla, 1972).
- O. Concepción and O. De Melo, “The versatile family of molybdenum oxides: Synthesis, properties, and recent applications,” *J. Phys.: Condens. Matter* **35**, 143002 (2023).
- C. V. Ramana, I. B. Troitskaia, V. V. Atuchin, M. Ramos, and D. Ferrer, “Electron microscopy characterization of hexagonal molybdenum trioxide (MoO₃) nanorods,” *J. Vac. Sci. Technol., A* **28**, 726–729 (2010).
- A. Guerfi and L. H. Dao, “Electrochromic molybdenum oxide thin films prepared by electrodeposition,” *J. Electrochem. Soc.* **136**, 2435–2436 (1989).
- V. S. Saji and C. Lee, “Molybdenum, molybdenum oxides, and their electrochemistry,” *ChemSusChem* **5**, 1146–1161 (2012).
- A. Bouzidi, N. Benramdane, H. Tabet-Derraz, C. Mathieu, B. Khelifa, and R. Desfeux, “Effect of substrate temperature on the structural and optical properties of MoO₃ thin films prepared by spray pyrolysis technique,” *Mater. Sci. Eng., B* **97**, 5–8 (2003).
- N. Wazir, C. Ding, X. Wang, X. Ye, X. Lingling, T. Lu, L. Wei, B. Zou, and R. Liu, “Comparative studies on two-dimensional (2D) rectangular and hexagonal molybdenum dioxide nanosheets with different thickness,” *Nanoscale Res. Lett.* **15**, 156 (2020).
- J. Sun, Q. Zheng, S. Cheng, H. Zhou, Y. Lai, and J. Yu, “Comparing molybdenum oxide thin films prepared by magnetron sputtering and thermal evaporation applied in organic solar cells,” *J. Mater. Sci.: Mater. Electron.* **27**, 3245–3249 (2016).
- M. Bivour, F. Zähringer, P. Ndione, and M. Hermle, “Sputter-deposited WO_x and MoO_x for hole selective contacts,” *Energy Procedia* **124**, 400–405 (2017).
- S. Berg and T. Nyberg, “Fundamental understanding and modeling of reactive sputtering processes,” *Thin Solid Films* **476**, 215–230 (2005).
- W. D. Sproul, D. J. Christie, and D. C. Carter, “Control of reactive sputtering processes,” *Thin Solid Films* **491**, 1–17 (2005).
- V. Bhosle, A. Tiwari, and J. Narayan, “Epitaxial growth and properties of MoO_x (2 < x < 2.75) films,” *J. Appl. Phys.* **97**, 083539 (2005).
- I. Petrov, L. Hultman, J.-E. Sundgren, and J. Greene, “Polycrystalline TiN films deposited by reactive bias magnetron sputtering: Effects of ion bombardment on resputtering rates, film composition, and microstructure,” *J. Vac. Sci. Technol., A* **10**, 265–272 (1992).
- J. Greene, J.-E. Sundgren, L. Hultman, I. Petrov, and D. Bergstrom, “Development of preferred orientation in polycrystalline TiN layers grown by ultrahigh vacuum reactive magnetron sputtering,” *Appl. Phys. Lett.* **67**, 2928–2930 (1995).
- H. Zaid, K. Tanaka, C. V. Ciobanu, J.-M. Yang, S. Kodambaka, and H. Kindlund, “Growth of elastically-stiff, nanostructured, high-entropy alloy nitride, (VNbTaMoW)N/Al₂O₃(0001) thin film,” *Scr. Mater.* **197**, 113813 (2021).
- I. Petrov, L. Hultman, U. Helmersson, J.-E. Sundgren, and J. Greene, “Microstructure modification of TiN by ion bombardment during reactive sputter deposition,” *Thin Solid Films* **169**, 299–314 (1989).
- K. Tanaka, M. E. Liao, A. Aleman, H. Zaid, M. S. Goorsky, and S. Kodambaka, “Growth of heterolayered [cubic-TaC (111)+rhombohedral-Ta₃C₂ (0001)] nanocomposite thin films on Al₂O₃ (0001),” *Acta Mater.* **204**, 116499 (2021).
- K. Tanaka, A. Aleman, H. Zaid, M. E. Liao, K. Hojo, Y. Wang, M. S. Goorsky, and S. Kodambaka, “Ultra-high vacuum dc magnetron sputter-deposition of 0001-textured trigonal α-Ta₂C/Al₂O₃ (0001) thin films,” *Materialia* **13**, 100838 (2020).
- G. Adabasi, A. Deshpande, K. Tanaka, J. Ancheta, E. Maldonado, M. Özdoğan, S. Kodambaka, and M. Z. Baykara, “Nanoscale friction of high entropy alloy sulfide thin films in comparison with molybdenum disulfide,” *Appl. Phys. Lett.* **123**, 261603 (2023).

- ³⁰K. Tanaka, H. Zaid, T. Aoki, A. Deshpande, K. Hojo, C. V. Ciobanu, and S. Kodambaka, "Growth of highly oriented (VNBMoTaW) S2 layers," *Nano Lett.* **24**, 493–500 (2024).
- ³¹A. Le Febvrier, L. Landälv, T. Liersch, D. Sandmark, P. Sandström, and P. Eklund, "An upgraded ultra-high vacuum magnetron-sputtering system for high-versatility and software-controlled deposition," *Vacuum* **187**, 110137 (2021).
- ³²M. Seah, "Summary of ISO/TC 201 standard: VII ISO 15472: 2001—Surface chemical analysis—X-ray photoelectron spectrometers—Calibration of energy scales," *Surf. Interface Anal.* **31**, 721–723 (2001).
- ³³ISO, "Surface chemical analysis—X-ray photoelectron spectrometers—Calibration of energy scales," Standard No. 15472:2010 (ISO, Geneva, Switzerland, 2010).
- ³⁴G. Greczynski and L. Hultman, "Binding energy referencing in x-ray photoelectron spectroscopy," *Nat. Rev. Mater.* **10**, 62–78 (2024).
- ³⁵M. Sook Oh, B. Seob Yang, J. Ho Lee, S. Ha Oh, U. Soo Lee, Y. Jang Kim, H. Joon Kim, and M. Soo Huh, "Improvement of electrical and optical properties of molybdenum oxide thin films by ultralow pressure sputtering method," *J. Vac. Sci. Technol., A* **30**(3), 2024 (2012).
- ³⁶A. L. Fernandes Cauduro, Z. E. Fabrim, M. Ahmadpour, P. F. Fichtner, S. Hassing, H. G. Rubahn, and M. Madsen, "Tuning the optoelectronic properties of amorphous MoO_x films by reactive sputtering," *Appl. Phys. Lett.* **106**(20), 2024 (2015).
- ³⁷S. Mohamed, O. Kappertz, J. Ngaruiya, T. L. Pedersen, R. Drese, and M. Wuttig, "Correlation between structure, stress and optical properties in direct current sputtered molybdenum oxide films," *Thin Solid Films* **429**, 135–143 (2003).
- ³⁸J. A. Kaduk, see <https://citeseerx.ist.psu.edu/document?repid=rep1&type=pdf&doi=590da22159193f2b9561d8f87d1a4c1752038b30> for "Maximizing the impact of your data: Applications of rietveld analysis to industrial problem solving" (1999).
- ³⁹H. Fujishita, M. Sato, S. Sato, and S. Hoshino, "Structure determination of low-dimensional conductor Mo₈O₂₃," *J. Solid State Chem.* **66**, 40–46 (1987).
- ⁴⁰T. Leisegang, A. Levin, J. Walter, and D. Meyer, "In situ x-ray analysis of MoO₃ reduction," *Cryst. Res. Technol.* **40**, 95–105 (2005).
- ⁴¹H.-K. Fun, P. Yang, M. Sasaki, M. Inoue, and H. Kadomatsu, "γ-Mo₄O₁₁," *Acta Crystallogr., Sect. C* **55**, 841–843 (1999).
- ⁴²J.-G. Choi and L. Thompson, "XPS study of as-prepared and reduced molybdenum oxides," *Appl. Surf. Sci.* **93**, 143–149 (1996).
- ⁴³D. O. Scanlon, G. W. Watson, D. Payne, G. Atkinson, R. Egdell, and D. Law, "Theoretical and experimental study of the electronic structures of MoO₃ and MoO₂," *J. Phys. Chem. C* **114**, 4636–4645 (2010).
- ⁴⁴H. Liu, X. Tian, Y. Liu, H. A. Munir, W. Hu, X. Fan, X. Liu, and L. Pang, "Synergistic polysulfides adsorption-conversion with Mo₂C–MoO₂ heterostructure for kinetically enhanced lithium-sulfur battery," *Energy Technol.* **12**, 2300820 (2024).
- ⁴⁵M. Anwar, C. Hogarth, and R. Bulpett, "Effect of substrate temperature and film thickness on the surface structure of some thin amorphous films of MoO₃ studied by x-ray photoelectron spectroscopy (ESCA)," *J. Mater. Sci.* **24**, 3087–3090 (1989).
- ⁴⁶L. Firment and A. Ferretti, "Stoichiometric and oxygen deficient MoO₃ (010) surfaces," *Surf. Sci.* **129**, 155–176 (1983).
- ⁴⁷D. Sheng, M. Zhang, X. Wang, S. Zhou, S. Fu, X. Liu, and Q. Zhang, "Carbon nanotubes embedded in α-MoO₃ nanoribbons for enhanced lithium-ion storage," *J. Mater. Sci.: Mater. Electron.* **33**, 11743–11752 (2022).
- ⁴⁸O. D. Melo, V. Torres-Costa, Y. González, A. Ruediger, C. D. Melo, J. Ghanbaja, D. Horwat, A. Escobosa, O. Concepción, G. Santana, and E. Ramos, "Interfacial strain defines the self-organization of epitaxial MoO₂ flakes and porous films on sapphire: Experiments and modelling," *Appl. Surf. Sci.* **514**, 145875 (2020).